Ionics (2014) 20:1343–1350
DOI 10.1007/s11581-014-1216-y

SHORT COMMUNICATION

Total conductivity in Sc-doped $LaTiO_{3+\delta}$ perovskites

M. Bradha · S. Hussain · Sujay Chakravarty · G. Amarendra · Anuradha Ashok

Received: 26 May 2014 / Revised: 28 June 2014 / Accepted: 18 July 2014 / Published online: 6 August 2014

Abstract A series of Sc-doped lanthanum titanate perovskites, $LaTi_{(1-x)}Sc_xO_{3+\delta}$ with x=0, 0.2, 0.25 and 0.3, was prepared by sol-gel method. All compositions were found to exhibit orthorhombic crystal structure. An increase in unit cell volume was observed for composition with x=0.2. The oxidation states of La^{3+}, Sc^{3+} and Ti^{3+} ions have been established using X-ray photoelectron spectroscopy (XPS). It is observed that an enhancement in total conductivity of $LaTiO_{3+\delta}$ perovskite is achieved only at lower doping concentration. A reverse effect is observed for higher dopant concentration.

Keywords Perovskites · SOFCs · Ionic conductivities · Diffusion

Introduction

Nowadays, inorganic oxides with high ionic conductivity are of great interest because of their potential applications as electrolytes in solid oxide fuel cells (SOFCs), gas sensors, gas separation membranes, etc. [1–5]. Recent developments in materials with high oxide ion conductivity have generated enormous interest in the design and development of new perovskite type oxides, because of their unique structural features suitable for aliovalent doping. Such doping creates vacancies in oxygen sublattice, which helps the migration of oxygen ions through the lattice [6, 7]. Among perovskites, $LaTiO_3$ is a promising material in diverse branches of applications such as electro-optical, piezoelectric, dielectric, ferroelectric, electrical conductivity and catalysis due to its unique properties [8]. Earlier, studies have been made to evaluate structural, electrical and morphological features of $LaTiO_3$ synthesized by various methods. It has been reported that doping in the A-site or B-site of this compound improves its overall properties [9–17]. Several authors have doped in the A-site divalent cations and studied its various properties [18–25]. Zang et al. reported the photocatalytic property by doping Cu at B-site of $LaTiO_3$, which was found to be highly effective for Fenton mechanism [26]. Literatures indicate that $LaScO_3$ is both proton and oxide ion conductor. The reason for high conductivity in scandate is a larger B-site ion, which will widen the lattice and create more space for the oxide ion to travel through the lattice [27–30]. Titanium exists in both trivalent and tetravalent oxidation states, and the ionic size of scandium is nearer to that of titanium when compared to other possible dopants such as Cu. Therefore, doping Sc in $LaTiO_{3+\delta}$ would not alter its crystal structure and thus affect its properties. The present work reports the incorporation of Sc^{3+} into $LaTiO_{3+\delta}$ to progress the total conductivity and structural properties of $LaTiO_{3+\delta}$ to make it more suitable for high-temperature applications. After structural and thermal analysis of the materials, their total conductivity is studied through impedance analysis.

M. Bradha · A. Ashok (✉)
Nanotech Research Facility, PSG Institute of Advanced Studies, Coimbatore, T.N 641004, India
e-mail: anu.machina@gmail.com

S. Hussain · S. Chakravarty · G. Amarendra
UGC-DAE CSR, Kalpakkam Node, Kokilamedu, T.N 603104, India

G. Amarendra
Indira Gandhi Centre for Atomic Research, Kalpakkam, T.N 603102, India

Experimental details

A series of $LaTi_{(1-x)}Sc_xO_{3+\delta}$ (x=0, 0.2, 0.25, 0.3) were synthesized by sol-gel method. High-purity (99.9 %) $La(NO_3)_3{\cdot}6H_2O$, $Sc(NO_3)_3{\cdot}6H_2O$ and $C_{12}H_{28}O_4Ti$ (Aldrich chemicals) were used as precursors. The precursor gel was prepared by using the following chemicals: 4.4 mmol

$La(NO_3)_3{\cdot}6H_2O$, 3 mmol $C_{12}H_{28}O_4Ti$ and 0.5 mmol $Sc(NO_3)_3{\cdot}6H_2O$ (for the perovskite composition with x=0.2) which were dissolved in 50 mL distilled water. After the formation of clear solution, 26 mmol citric acid and 5 mmol polyethylene glycol were added and the solution was heated to 60 °C with continuous stirring for 8 h to obtain a gel. Similarly for other compositions, calculated amounts of precursors were taken and reactions were carried out. The gel was heated to 120 °C in a hot air oven to get a brown porous solid which was calcined at 800 °C for 2 h to obtain a white powder of $LaTi_{0.8}Sc_{0.2}O_{3+\delta}$. The calcined powder of each composition was ground into a fine powder in an agate mortar and then uniaxially pressed into cylindrical pellet of 10 mm diameter and 1.6 mm thickness using hydraulic press by applying a pressure of 1,800 kg/cm^2. Subsequently, the pellets were sintered at 1,200 °C for 10 h in air atmosphere and further characterizations and conductivity measurements were carried out.

The precursors in the form of dried gel were subjected to thermogravimetry/differential scanning calorimetry (TG/DSC) performed using NETZSCH STA 449F3 in static air atmosphere from room temperature to 1,000 °C at a heating rate of 10 °C min^{-1} to determine the temperature of formation of perovskite oxide phase. The phase identification and structural characterization of the perovskites was carried out by X-ray diffraction (XRD) using PHILIPS X-ray Diffractometer with CuKα radiation (λ=1.540598 Å) with 2θ ranging from 10° to 60° at an acquisition rate of 0.02°/s. Unit cell dimensions of the crystal structure were refined by Rietveld (Le-Bail fitting) method using X-pert HighScore Plus program. The microstructure of the sintered pellets was recorded using scanning electron microscopy (SEM) in Carl-Zeiss Auriga SEM in secondary emission mode. Oxidation states of the perovskites were analysed using by X-ray photoelectron spectroscopy (XPS, Specs-phoibos analyser) with a monochromatized Al K X-ray source of 1,486.58 eV. Total conductivity of the perovskites was studied through impedance measurement using a computer controlled impedance analyser HIOKI 3532 LCR HITESTER in the frequency ranging from 50 Hz to 10 MHz and at a temperature range of 30–650 °C. For better ohmic contact, high-temperature curing silver paste was applied on both faces of the pellet.

Results and discussion

Formation process of $LaTi_{(1-x)}Sc_xO_{3+\delta}$ (x=0, 0.2, 0.25, 0.3) using TG/DSC

Thermal analysis results of all the dried gels obtained during the synthesis of undoped and Sc-doped $LaTiO_{3+\delta}$ perovskites are shown in Fig. 1. Figure 1a shows the thermal analysis of undoped $LaTiO_{3+\delta}$. The curves depict the weight loss profiles that occur in several stages. The weight loss observed in the range between room temperature and 300 °C is due to the removal of adsorbed and structural water from the sample. The second stage between 300 and 500 °C is accompanied by an endothermic peak at the DSC curve with weight loss that is due to the decomposition of nitrates and citrate complexes. The third stage in the range from 500 to 800 °C, and its accompanying weight loss represents the loss of organics and carbon dioxide from metal oxides. This is also represented by an endothermic peak at the DSC curve. The fourth stage in the range of 800–1,000 °C with weight loss is attributed to the oxygen loss and formation of perovskite phase and the structure variation in TiO_6 octahedron under higher calcination temperatures [31]. After doping Sc with different concentrations in the B-site as shown in Fig. 1b–d, no major changes were observed in TG/DSC curve. This indicates that all samples can be calcined at 800 °C for 2 h to obtain an oxygen-deficient perovskite phase.

Powder X-ray diffraction and structure

Powder XRD patterns of the sintered perovskites, $LaTi_{(1-x)}Sc_xO_{3+\delta}$ (x=0, 0.2, 0.25, 0.3), are shown in Fig. 2a. Well-defined peaks indicate the crystalline nature of the synthesized compounds without any impure phase. The characteristic peaks observed in these patterns are indexed according to an orthorhombic crystal structure having space group Pnma (62). The refined unit cell parameters are listed in Table 1. The refinement plot is shown in Fig. 2b. Ionic radii of trivalent Ti and Sc for octahedral coordination are 0.67 and 0.745 Å, respectively [32]. As shown in the inset in Fig. 2a, with increase of Sc concentration, slight shifts in the peak positions due to change in cell dimension can be observed. We observe a gradual decrease in lengths of a-axis and increase in b- and c-axes of the orthorhombic unit cell with increase in dopant concentration. We also observe a substantial decrease in peak intensities (as shown in the inset for the 221 plane) for doped perovskites. This may be due to the substitution of dopants among certain preferred crystallographic axes or planes and resulting octahedral tilting/deformation. The overall effect can be observed in the unit cell volume calculated from the experimentally obtained cell dimensions. Maximum cell volume is observed for the composition with x=0.2. As observed from our results, this may be the solubility limit and doping Sc beyond this level may result in small amount of secondary phases which can be undetectable in XRD.

Scanning electron microscopy studies

SEM micrographs of the sintered pellets are shown in Fig. 3. Figure 3a shows the morphology of the undoped $LaTiO_{3+\delta}$ perovskite. Figure 3b–d shows micrographs of the doped

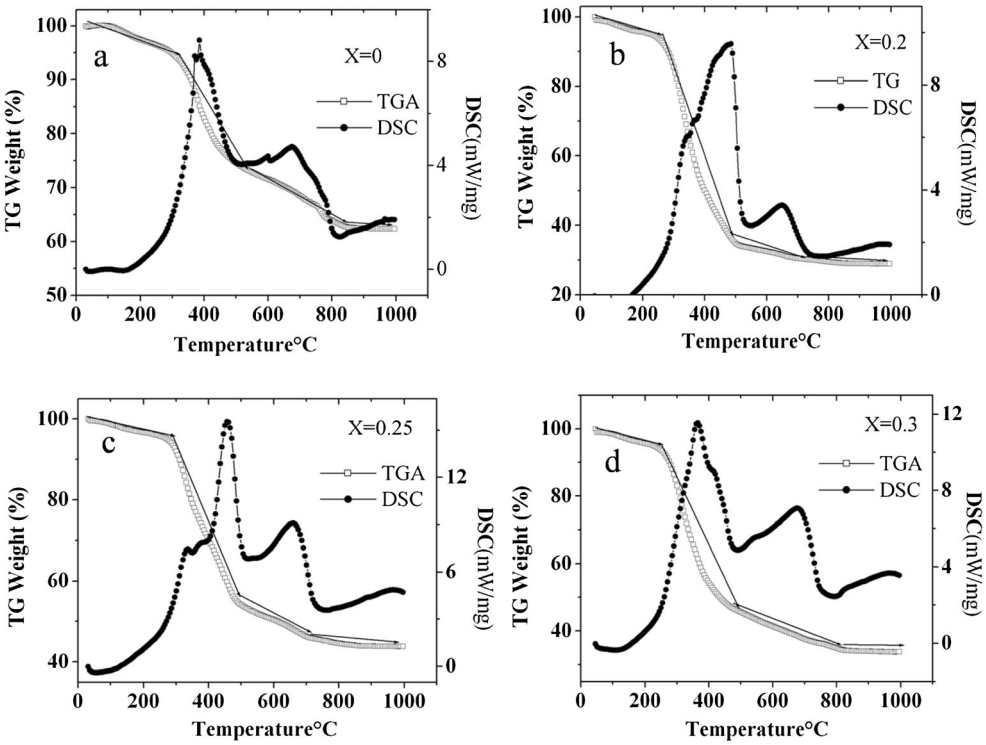

Fig. 1 TG/DSC data of $LaTi_{(1-x)}Sc_xO_{3+\delta}$ synthesized by sol-gel method for various compositions: **a** x=0, **b** x=0.2, **c** x=0.25 and **d** x=0.3

$LaTi_{(1-x)}Sc_xO_{3+\delta}$ for x=0.2, 0.25 and 0.3, respectively. Figure 3e represents a representative lower-magnification image (for x=0.2). A similar morphology was exhibited by all the other compositions. Micrographs reveal that the pellets are well sintered and have defined grains with distinct boundaries but with irregular morphology. The surface morphology of the samples indicates that ordered grains of unequal size are distributed throughout the sample with very small porosity. From the figure, it can be seen that the surface of each particle is composed of smaller particles. Extended contact to high temperature has resulted in agglomeration and fusion of the particles which appear as larger grains in microstructural images. No significant change in the morphology was observed due to different concentrations of doping.

X-ray photoelectron spectroscopy studies

The oxidation states of lanthanum, titanium and scandium in the perovskite $LaTi_{(1-x)}Sc_xO_{3+\delta}$ with x=0.2 were studied by using XPS. XPS spectra are shown in Fig. 4. Figure 4a represents La 3d state, Fig. 4b shows Ti 2p state, Fig. 4c shows Sc 2p state and Fig. 4d shows the O 1 s state of the perovskite. The binding energy of La 3d is 853 eV. Because of the shake-up effect, we observe two peaks in La $3d_{3/2}$ spectra from 853.3 to 849.5 eV. The presence of small satellite peaks in the spectra is due to the suborbitals in 3d orbital. From the data, it is clear that for La, the La 3d peaks that appear at 853.3–849.5 eV ($3d_{3/2}$) correspond to La^{3+}. It has been observed that the binding energy splitting between the components of both La $3d_{3/2}$ and La $3d_{5/2}$ lines is ~4.1 eV in $La_2Ti_2O_7$, $LaNbO_4$ and $Ca_4LaO(BO_3)_3$ crystals, and this value is higher than ~3.5 eV in La_2O_3 [33–35]. The presence of satellite peak La 3d is due to the monopole excitation arising from a change in the screening of the valence electrons upon the removal of a core electron. Similar phenomenon was reported earlier by Miao et al. [36]. In our sample, the Ti 2p located at binding energies of 463.2 and 458.2 eV, respectively, indicates the presence of Ti^{3+}. After sintering at high temperature, there is a possible transfomation tendency from Ti^{4+} to Ti^{3+} with a peak shift. This suggests that the Ti ions on the surface of the sample are trivalent. Similar studies for Ti 2p spectra of TiO_4 and TiO_7 were reported by Rao et al. [37]. Figure 4c represents the Sc 2p spectra. In the Sc 2p spectra, the satellite peaks observed on the high-binding energy side of the main peak by about 4.5 eV can be interpreted in terms Sc existing with the oxidation state 3+. The O 1 s spectra (Fig. 4d) shows the maximum binding energy at 529.82 eV. When lanthanum and titanium interact with oxygen, valence electrons are transferred from metals to oxygen atoms with variation in electrical screening of the inner shells. Thus, binding energies of the inner electrons of metal ions increase with synchronous decrease in the binding energy of O 1-level oxygen ions. The shift in binding energies is because of lanthanum- and titanium-bearing oxides. In the O 1 s spectra, the appearance of a low tail at higher binding energy confirms the oxygen deficiency of perovskite [38].

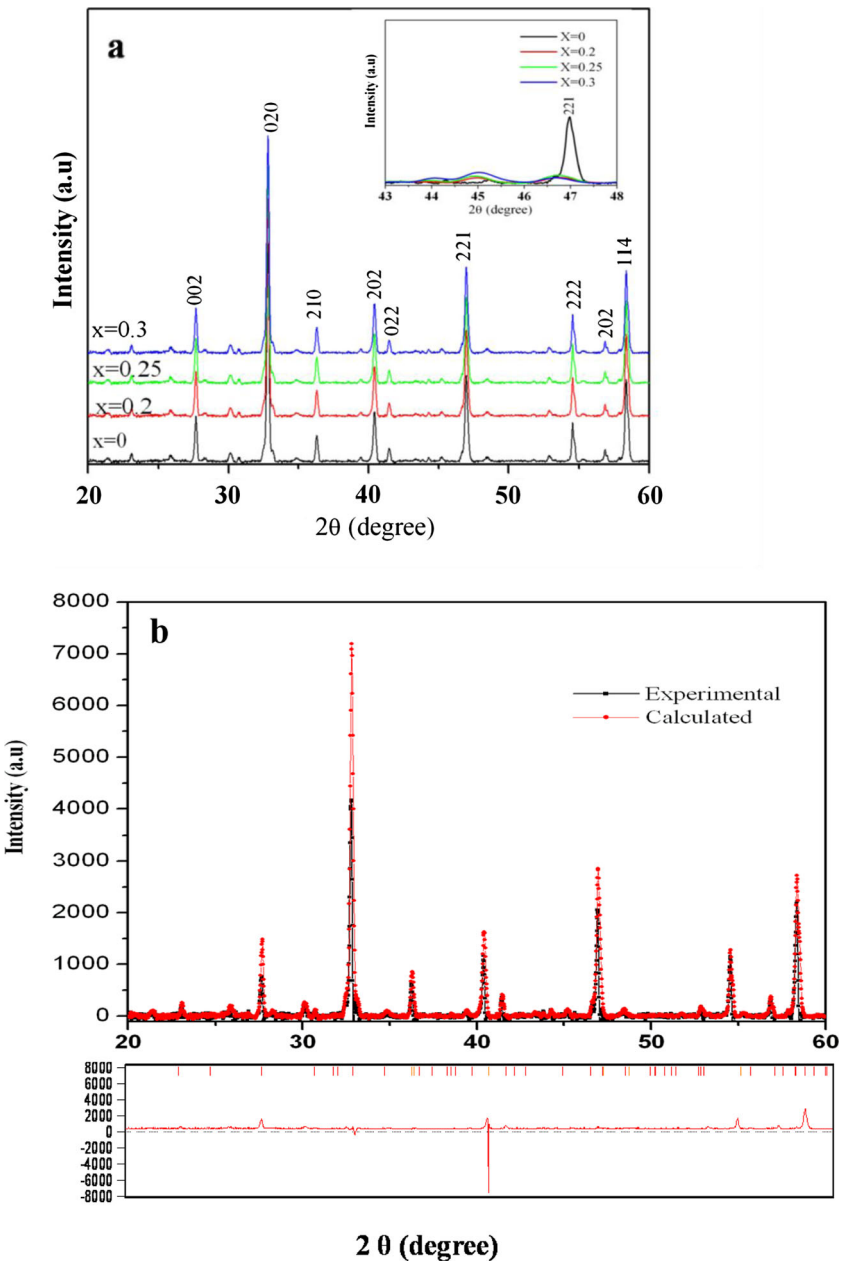

Fig. 2 Powder XRD patterns of sintered $LaTi_{(1-x)}Sc_xO_{3+\delta}$ (x=0, 0.2, 0.25, 0.3)

Table 1 Refined lattice parameters, total conductivity and activation energies for the undoped and doped $LaTi_{(1-x)}Sc_xO_{3+\delta}$ (x=0, 0.2, 0.25, 0.3) perovskites

Composition	Lattice parameters (Å)			Cell volumes (Å^3)	Total conductivity at 650 °C (S/cm)	Activation energy (eV)
	a	*b*	*c*			
$LaTi_{(1-x)}Sc_xO_{3+\delta}$ (x=0)	5.84	5.6	7.7	255.0464	9.81×10^{-4}	0.42±0.01
$LaTi_{(1-x)}Sc_xO_{3+\delta}$ (x=0.2)	5.82	5.7	8.00	265.392	4.56×10^{-3}	0.62±0.66
$LaTi_{(1-x)}Sc_xO_{3+\delta}$ (x=0.25)	5.80	5.75	7.90	263.465	4.56×10^{-5}	0.35±0.91
$LaTi_{(1-x)}Sc_xO_{3+\delta}$ (x=0.3)	5.80	5.76	7.90	263.923	9.60×10^{-5}	0.24±0.20

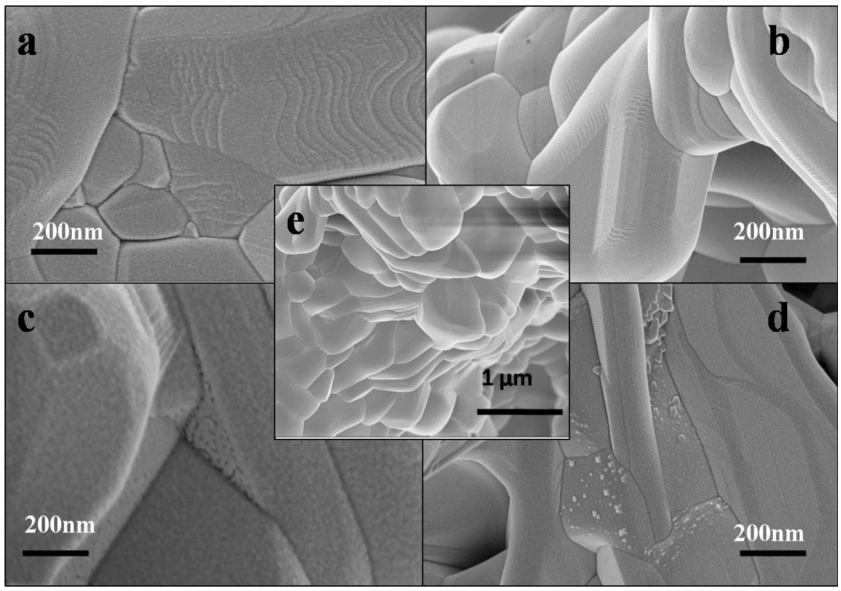

Fig. 3 SEM images of the sintered $LaTiO_{3+\delta}$ and $LaTi_{(1-x)}Sc_xO_{3+\delta}$. **a** x=0, **b** x=0.2, **c** x=0.25, **d** x=0.3 **e** Image corresponding to the composition with x = 0.2 at lower magnification

Total conductivity measurements

The total charge transport properties were measured as a function of frequency and temperature using impedance spectroscopy over a wide range of frequency (50 Hz to 10 MHz) within the temperature range 30–650 °C. Figure 5 shows the Cole-Cole plot of $LaTi_{(1-x)}Sc_xO_{3+\delta}$ (x=0, 0.2, 0.25, 0.3) at 650 °C. The experimental semicircle is related to ionic conduction in both bulk and grain boundary. Contribution from the electrode is not observed at lower frequencies. The value of resistivity can be determined from the intercepts of the semicircle on the x-axis. It can be observed from Fig. 5b that after doping Sc, the resistivity decreases when compared with the undoped perovskite Fig. 5a. The total DC conductivity is calculated using the following equation:

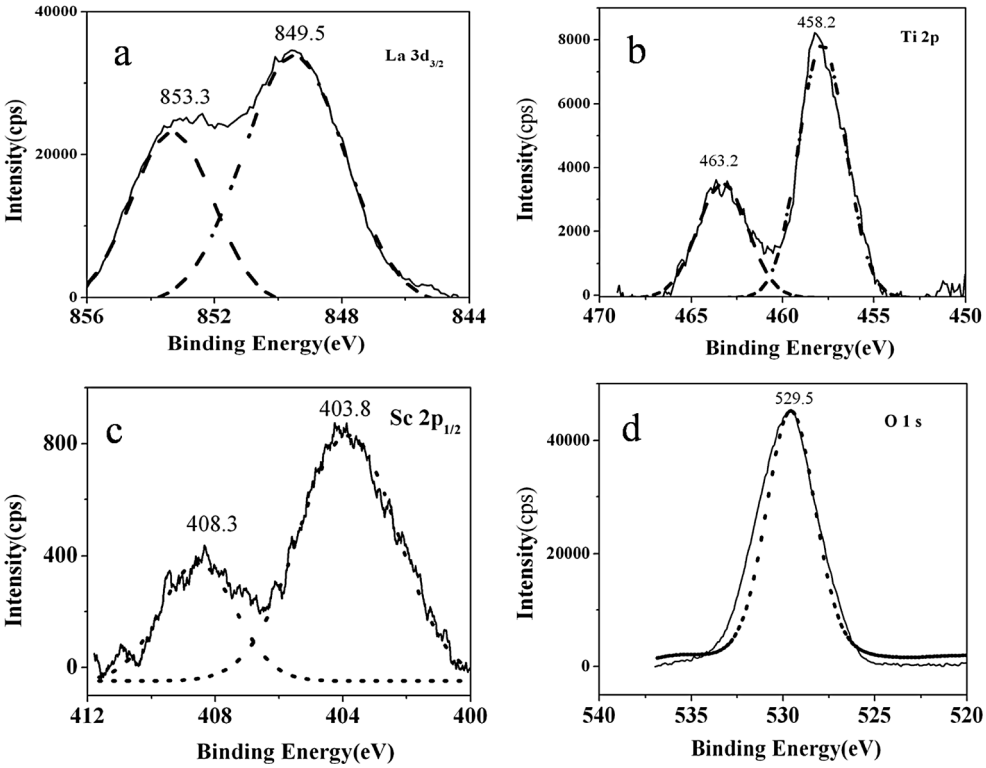

Fig. 4 XPS spectra of the surface of sintered pellet $LaTi_{(1-x)}Sc_xO_{3+\delta}$ (x=0.2), depicting **a** La 3d, **b** Ti 2p, **c** Sc 2p and **d** O 1 s peaks

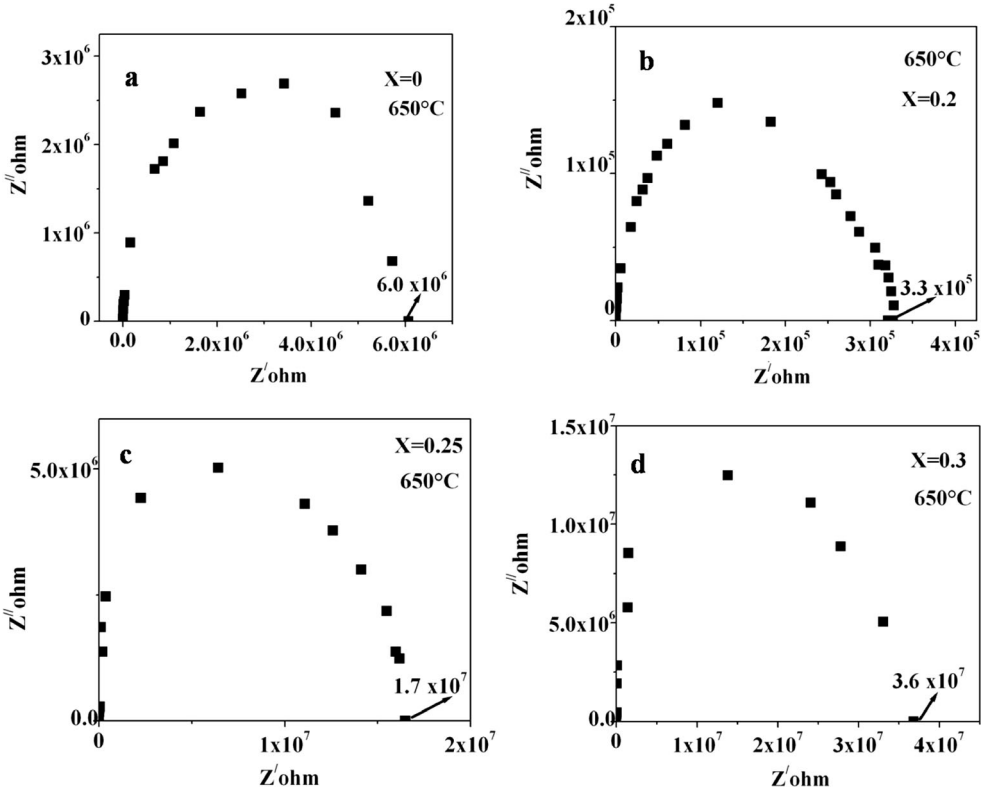

Fig. 5 Cole-Cole plot of $LaTi_{(1-x)}Sc_xO_{3+\delta}$ at 650 °C, **a** x=0, **b** x=0.2, **c** x=0.25 and **d** x=0.3

$$\sigma = \frac{l}{Rb\,A}\,\mathrm{S\ cm^{-1}} \tag{1}$$

where R_b is the resistance of the sample, l is the thickness of the sample and A is the area of the sample.

Figure 6 shows the total conductivity (log σ) as a function of inverse of absolute temperature (1,000/T). The nature of variation is almost linear in accordance with Arrhenius equation

$$\sigma = \sigma_0 \exp(-E_a/K_B T) \tag{2}$$

where E_a is the activation energy, T is the absolute temperature and σ_0 is the pre-exponential factor. It is obvious from the plot that the conductivity increases with the increase in temperature. This indicates negative temperature coefficient of resistance (NTCR) behaviour of the samples. The activation energy of the carriers for conduction process is calculated using Eq. (2). Activation energy and total conductivity at 650 °C for all the perovskites studied in this work are given in Table 1.

The diffusion coefficient of carriers in $LaTi_{(1-x)}Sc_xO_{3+\delta}$ (x=0, 0.2, 0.25, 0.3) is calculated under different temperatures ranging from 520 to 650 °C. Figure 7 shows the variation of diffusion coefficient of carriers as a function of reciprocal

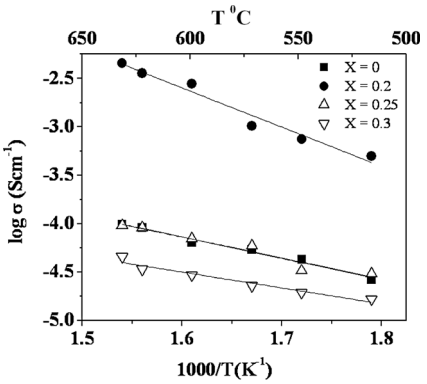

Fig. 6 Variation of log conductivity with respect to reciprocal temperature for $LaTi_{(1-x)}Sc_xO_{3+\delta}$ (x=0, 0.2, 0.25, 0.3)

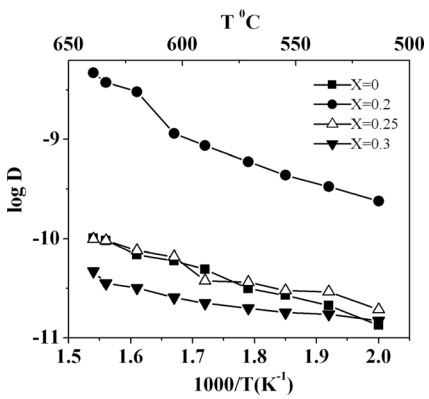

Fig. 7 Variation of log diffusion coefficient (D) with respect to reciprocal temperature for $LaTi_{(1-x)}Sc_xO_{3+\delta}$ (x=0, 0.2, 0.25, 0.3)

temperature. The diffusion coefficient is calculated using the formula:

$$D = \frac{\sigma KBT}{Ne^2} \quad (3)$$

where σ is the electrical conductivity, K_B is Boltzman constant, T is the temperature, N is the number of atoms in an unit cell and e is the electronic charge [39]. From the figure, it is clear that after doping trivalent cations in the Ti site, there is an increase in diffusion coefficient with the increase in temperature which brings about enhanced mobility of the carriers. Consequently, it is assumed that at higher temperature, ionic mobility is higher. The inherent oxygen vacancies that can exist in unit cells due to various levels of doping and sintering conditions can also contribute to mobility and alter the diffusion coefficient.

Our results indicate that doping Sc^{3+} at Ti^{3+} site has altered the total conductivity of $LaTiO_{3+\delta}$. It can be observed that conductivity attains a maximum for the composition x=0.2 and, further, a decrease is observed for x=0.25 and x=0.3. The calculated unit cell volume from cell dimensions obtained through XRD analysis (Table 1) shows that the composition with x=0.2 has the maximum value. The perovskite with the same composition also shows the maximum diffusion coefficient and highest total conductivity at all measured temperatures. From Table 1, it is evident that the perovskite with composition x=0.2 has higher activation energy (0.62 eV) and exhibited the highest conductivity of 4.56×10^{-3} S/cm, which is due to the predominant ionic conductivity at higher temperature. Since the conductivity is temperature dependent, it is assumed that ions are responsible for the conductivity at higher temperature. This type of behaviour was reported by Stevenson et al., [40] in nonstoichiomertric perovskites. Based on XPS results (which conveys that both are trivalent), it is evident that doping Sc in the position of Ti does not create any additional oxygen vacancies, since after sintering at high temperature, Ti will no longer exist as tetravalent. Therefore, the possible reason for enhanced conductivity in the perovskite with composition x=0.2 might be enhanced mobility of the carriers due to larger cell volume which involves localized hopping with either rotation or translation of the mobile species [7]. When compared with the conductivity data using other dopants than Sc at B-site of $LaTiO_{3-\delta}$ available in literature [41], Sc doping (up to x=0.2) is more effective in enhancing the total conductivity at high temperature when compared to other dopants studied so far.

Conclusion

$LaTi_{(1-x)}Sc_xO_{3-\delta}$ (x=0, 0.2, 0.25, 0.3) perovskites were successfully synthesized using sol-gel method. XRD confirmed a single phase showing an orthorhombic structure. A similar microstructure with fine grain size was observed in all the perovskites. XPS data confirmed the presence of Sc in the material and the valence states for La^{3+}, Ti^{3+} and Sc^{3+}, related to oxygen-deficient perovskite structure. This investigation shows that among the studied compositions, doping Sc on $LaTiO_{3+\delta}$ perovskites can successfully improve the total conductivity only up to a certain dopant concentration (x=0.2), beyond which a reverse effect occurs.

Acknowledgments The authors (Bradha. M and Anuradha Ashok) wish to acknowledge UGC-DAE CSR for providing financial support to carry out this research work. We acknowledge Bharathiar University, Coimbatore, for extending the facility for Ac conductivity measurements and IIT Madras for XRD measurements.

References

1. Kinoshita K (1992) Electrochemical oxygen technology. Wiley, New York
2. Steele BCH (1994) Oxygen transport and exchange in oxide ceramics J Power Sources 49:1
3. Logan AD, Shelef M (1996) Oxygen availability in mixed cerium/praseodymium oxides and the effect of noble metals J Mater Res 11:1960
4. Knauth P, Tuller HL (1999) Nonstoichiometry and relaxation kinetics of nanocrystalline mixed praseodymium – Cerium oxide $Pr_{0.7}Ce_{0.3}O_{2-x}$ J Eur Ceram Soc 19:831
5. Narula CK, Haack LP, Chun W, Jen HW, Graham GW (1999) Single-phase PrO_y-ZrO_2 materials and their oxygen storage capacity: A comparison with single-phase CeO_2-ZrO_2, PrO_y-CeO_2, and PrO_y-CeO_2-ZrO_2 J Phys Chem B 103:3634
6. Bonanos N, Knight KS, Ellis B (1995) Perovskite solid electrolytes: Structure, transport properties and fuel cell applications, Solid State Ionics 79:161
7. Kendall KR, Navas C, Tomas JK, zur Loye HC (1995) Recent developments in perovskite-based oxide ion conductors Solid State Ionics 82:215–223
8. Fasquelle D, Carru JC, Le Gendre L, Le Paven C, Pinel J, Chevire F, Tessier F, Marchand R (2005) Lanthanum titanate ceramics: Electrical characterizations in large temperature and frequency ranges J Eur Ceram Soc 25:2085–2088
9. Kestigian M, Ward R (1955) The Lanthanum-Titanium-Oxygen System J Am Chem Soc 77(23):6199–6200
10. Roth RS (1956) Pyrochlore-type compounds containing double oxides of trivalent and tetravalent ion J Res Natl Bur Stand 56:17
11. Fuierer PA, Newnham RE (1991) $La_2Ti_2O_7$ ceramics J Am Ceram Soc 74:2876
12. Skapin SD, Kolar D, Suvorov D (1999) Phase equilibria and solid solution relationships in the La_2O_3-TiO_2-ZrO_2 system Solid State Sci 1:245
13. Gasperin M (1975) Dititanate de Lanthane Acta Crystallogr B 31:2129
14. S. Havelia, K.R. Balasubramaniam, S. Spurgeon, F. Cormack, P.A. Salvador (2008) Growth of $La_2Ti_2O_7$ and $LaTiO_3$ thin films using pulsed laser deposition, Journal of Crystal Growth 310 1985–1990
15. Prasadarao AV, Selvaraj U, Komarneni S, Bhalla AS (1991) Grain orientation in sol-gel derived $Ln_2Ti_2O_7$ ceramics (Ln= La,Nd) Mater Lett 12:306
16. Ohtomo A, Muller DA, Grazul JL, Hwang HY (2002) Epitaxial growth and electronic structure of films Appl Phys Lett 80:3922

17. Osborn R, Aronson MC, Goremychkin EA, Greedan JE (1996) The magnetic response at the metal–insulator transition in $La_{1-x}Sr_xTiO_3$ J Appl Phys 79:6432
18. Kim K, Kwon YW, Norton DP, Christen DK, Budai JD, Sales BC, Chisholm MF, Cantoni C, Marken K (2003) Epitaxial (La,Sr)TiO_3 as a conductive buffer for high temperature superconducting coated conductors Solid State Electron 47:2177
19. Abe M, Uchino K (1974) X-ray study of the deficient perovskite $La_{2/3}TiO_3$ Mater Res Bull 9:147
20. MacChesney JB, Gallagher PK, Dimarcello FV (1963) Stabilized barium titanate ceramics for capacitor dielectrics J Am Ceram Soc 46:197
21. Tien TY, Cross LE (1967) Dielectric relaxation in strontium titanate solid solutions containing lanthania J Appl Phys 6:459
22. Kim IS, Jung WH, Inaguma Y, Nakamura T, Ioth M (1995) Dielectric properties of a-site deficient perovskite-type lanthanum-calcium-titanium oxide solid solution system [(1-x)$La_{2/3}TiO_{3-x}CaTiO_3$(0.1≤x ≤ 0.96)] Mater Res Bull 30:307
23. G. Campet, J. Claverie (1983) Influence of Cr^{3+} doping on photoelectronic processes of La2Ti207 pyrochlore and $La_{2/3}TiO_{3-x}$ perovskite anodes, .I. Phys. Chem. Solids. 44, 925–929.
24. Ali R, Yashima M, Tanaka M, Yoshioka H, Mori T, Sasaki S (2002) High-temperature synchrotron x-ray powder diffraction study of the orthorhombic-tetragonal phase transition in $La_{0.63}$ ($Ti_{0.92}$, $Nb_{0.08}$)O_3 J Solid State Chem 164:51–59
25. Vashook V, Vasylechko L, Knapp M, Ullmann H, Guth U (2003) Lanthanum doped calcium titanates: synthesis, crystal structure, thermal expansion and transport properties J Alloys Compd 354:13–23
26. Zhang L, Nie, Hu C, Qu J (2012) Enhanced Fenton degradation of Rhodamine B over nanoscaled Cu-doped $LaTiO_3$ Perovskite Appl Catal B Environ 125:418–424
27. Kilner JA, Brook RJ (1982) A study of oxygen ion conductivity in doped non-stoichiometric oxides Solid State Ionics 6:237–252
28. Sammells AF, Cook RL, White JH, Osborne JJ, MacDuff RC (1992) Rational selection of advanced solid electrolytes for intermediate fuel cells Solid State Ionics 52:111–123
29. Cook RL, Sammells AF (1991) On the systematic selection of perovskite solid electrolytes for intermediate temperature fuel cells Solid State Ionics 45:311–321
30. Lybye D, Bonanos N (1999) Proton and oxide ion conductivity of doped $LaScO_3$ Solid State Ionics 125:339–344
31. Hou WM, Ku Y (2011) Synthesis and characterization of $La_2Ti_2O_7$ employed for photocatalytic degradation of reactive red 22 dyestuff in aques solution J Alloys Compd 509:5913–5918
32. Shannon RD (1976) Revised effective ionic radii and systematic studies of interatomie distances in halides and chaleogenides Acta Crystallogr A32:751–767
33. Nelson AJ, Adams JJ, Schaffers K. J (2003) Photoemission investigation of the electronic structure of lanthanum–calcium oxoborate Appl Phys 94:7493–7495
34. Suga S, Imada S, Muro T, Fukawa T, Shishidou T, Tokura Y, Moritomo Y, Miyahara T. J (1996) La 4d and Mn core absorption magnetic circular dichroism, XPS and inverse photoemission spectroscopy of $La_{1-x}Sr_xMnO_3$ Electron Spectrosc Relat Phenom 78: 283–286
35. Teterin Yu A, Baev AS (1987) X-ray photoelectron spectroscopy of lanthanide compounds (Moscow: CNII atom in form) (in Russian)
36. Miao JP, Li LP, Liu HJ, Xu DP, Lu Z, Song Y-B, Su W-H, Zheng Y-G (2000) Structure characteristics and valence state study for $La_{1-x}Na_xTiO_3$ synthesized under high-pressure and high-temperature conditions Mater Lett 42:1–6
37. Rao CNR, Sarma DD (1982) Study of Electron States of Solids by Techniques of Electron Spectroscopy J Solid State Chem 45:14–39
38. Rojas ML, Fierro JLG (1990) Synthesis and characterization of $LaTi_{1-x}Cu_xO_3$ compounds J Solid State Chem 89:299–307
39. Hemada OM, Saadaway ME (2003) Effect of gamma irradiation on the structural properties and diffusion coefficient in Co–Zn ferrite J Magn Magn Mater 256:63
40. Stevenson JW, Hasinska K, Canfield NL, Armstrong TR (2000) Influence of Cobalt and Iron Additions on the Electrical and Thermal Properties of (La,Sr)(Ga,Mg)$O_{3-\delta}$ J Electrochem Soc 147:3213
41. Du Z, Zhao H, Zhou X, Xie Z, Zhang C (2013) Electrical conductivity and cell performance of $La_{0.3}Sr_{0.7}Ti_{1-x}Cr_xO_{3-\delta}$ perovskite oxides used as anode and interconnect material for SOFCs Int J Hydrog Energy 38:1068–1073